JMEPEG (2015) 24:545–555
DOI: 10.1007/s11665-014-1311-2

1059-9495/$19.00

Effect of Thermomechanical Treatment on the Environmentally Induced Cracking Behavior of AA7075 Alloy

Rahul Ghosh, A. Venugopal, P. Sankaravelayudham, Rajiv Panda, S.C. Sharma, Koshy M. George, and V.S. Raja

(Submitted June 6, 2014; in revised form November 2, 2014; published online December 2, 2014)

The influence of thermomechanical treatment on the stress corrosion cracking behavior of AA7075 aluminum alloy forgings was examined in 3.5% NaCl solution by varying the extent of thermomechanical working imparted to each of the conditions. The results show that inadequate working during billet processing resulted in inferior corrosion and mechanical properties. However, more working with intermediate pre-heating stages also led to precipitation of coarse particles resulting in lowering of mechanical properties marginally and a significant reduction in the general/pitting corrosion resistance. The results obtained in the present study indicate that optimum working with controlled pre-heating levels is needed during forging to achieve the desired properties. It is also demonstrated that AA7075 in the over aged condition does not show any environmental cracking susceptibility in spite of the microstructural variations in terms of size and volume fraction of the precipitates. However, the above microstructural variations definitely affected the pitting corrosion and mechanical properties significantly and hence a strict control over the working and pre-heating stages during billet processing is suggested.

Keywords AA7075, stress corrosion cracking (SCC), thermomechanical treatment

1. Introduction

Aluminum alloy such as AA7075 is a precipitation-hardenable alloy widely used in the aircraft and aerospace industries owing to its high strength to weight ratio, light weight, and good stress corrosion cracking (SCC) resistance especially in the over aged (T7) condition. The high SCC resistance in the T7 condition was shown to be due to change in the size and distribution of strengthening precipitates ($MgZn_2$) (Ref 1-3). In spite of the significant improvement in the SCC resistance, localized corrosion such as pitting remains a problem in high strength aluminum alloys in view of the differences in electrochemical of the precipitates over the matrix aluminum (Ref 4-9). These precipitates can be either anodic or cathodic with respect to the matrix aluminum. In addition to the strengthening precipitates, elements such as Cu and Fe form intermetallic phases such as Al_7Cu_2Fe, $(Al, Cu)_6$ (Fe, Cu), and Mg_2Si are highly detrimental to the localized corrosion resistance of commercial aluminum alloys. Hence, several studies were directed toward understanding the localized corrosion of high strength aluminum alloys containing the above phases. Such localized corrosion pits caused by the above intermetallic phases have been reported to be the initiation sites for fatigue crack resulting in premature failure of AA7075 aluminum alloys (Ref 10).

In the aerospace industry, the components are generally manufactured by hot rolling, forging, or extrusion processes. Manufacturing of components through forging involves thermomechanical working in perpendicular directions alternately to arrive at a desired three-dimensional shape. AA7075 alloy in T7352 condition is used in several control components of launch vehicles such as parts (valves/sleeves) of a conduit line for filling the liquid chemical to its storage tank. The strain rate and temperature are important as they strongly influence microstructure, crystallographic texture, and corrosion properties of the resultant forging (Ref 11, 12). The extent of working during hot deformation and the rate of cooling sometimes may lead to heterogeneous microstructure which may also influence the corrosion especially in the case of large forgings. The present study is aimed at understanding the effect of varying thermomechanical working on the variations in microstructure and its influence on the mechanical, corrosion, and environmental cracking resistance of AA7075 aluminum alloy forgings.

Rahul Ghosh, P. Sankaravelayudham, and **Rajiv Panda**, Materials Management Division, Vikram Sarabhai Space Centre, Thiruvananthapuram 695 022, India; **A. Venugopal** and **S.C. Sharma**, Materials and Metallurgy Group, Vikram Sarabhai Space Centre, Thiruvananthapuram 695 022, India; **Koshy M. George**, Materials and Mechanical Entity, Vikram Sarabhai Space Centre, Thiruvananthapuram 695 022, India; and **V.S. Raja**, Department of Metallurgical Engineering and Materials Science, Indian Institute of Technology, Bombay, Mumbai 400 076, India. Contact e-mail: arjun_venu@hotmail.com.

2. Experimental

2.1 Material

AA7075 homogenized billets (dia. 245 × 95 mm) realized at M/s Hindalco-Almex, Aurangabad, India was used as an input material for the present work having nominal composition

around Al-5.56 Zn-2.52 Mg-1.51 Cu-0.18 Cr-0.15 Fe-0.103 Si (wt.%). Typical microstructure of the homogenized billet in the as-received condition is shown in Fig. 1 having average grain size of 130 μm. The homogenized billets were further processed through a series of forging operations after subjecting to hot working in perpendicular directions alternately, with intermediate pre-heating to the required dimensions (size 95 × 95 × 245 mm) shown in Fig. 2. In this paper, each stage is represented by a terminology as TP1, TP2, and TP3, respectively, in the order of increased thermomechanical working imparted. These experimental samples were worked at different levels and will be referred as less worked (TP1), intermediately worked (TP2), and sufficiently worked (TP3) throughout this paper.

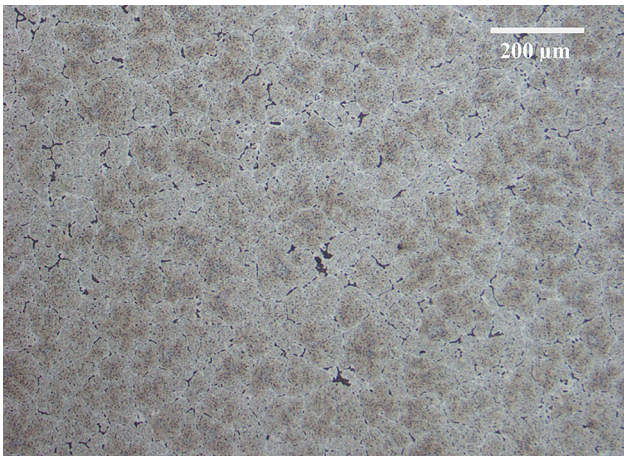

Fig. 1 Optical micrograph of the as-received AA7075 homogenized cast billet

The forging operations were carried out using a 3.15 T hammer at a deformation velocity between 1.5 and 2.0 m s^{-1} and an average strain rate of 5-6 s^{-1}. The resulting forged material was finally heat treated to T7352 condition (solution treated at 470 °C for 4.5 h + Quenching in water + stress relieved by compression followed by dual step aging at 107 °C-7 h and 177 °C-7 h and air cooled).

The tensile specimens were fabricated by cutting the specimen coupons in the transverse direction of the forgings. Sub-scale tensile specimens of gage diameter 6.25 mm were used after detailed radiographic examination and tested at a strain rate of 10^{-3} s^{-1}. For SCC tests, subsize tensile specimens as per ASTM G129 were used.

2.2 Microstructures

Optical microscopy (OM) and scanning electron microscopy (SEM) coupled with Energy dispersive x-ray spectroscopy (EDS) were used for microstructure and elemental analysis of the forged alloy samples, respectively. The samples were sectioned and polished down to 5 μm alumina finish followed by etching in freshly prepared Keller's reagent (5 ml HNO_3, 3 ml HCl, 2 ml HF, and 190 ml distilled water) and examined under an Olympus make GS 71 optical microscope. Elemental analysis was carried out using a Carl Zeiss make EVO-50 environmental scanning electron microscope. The fractured samples were examined under a SEM to observe the change in the fracture morphology as a result of the exposure to the NaCl environment.

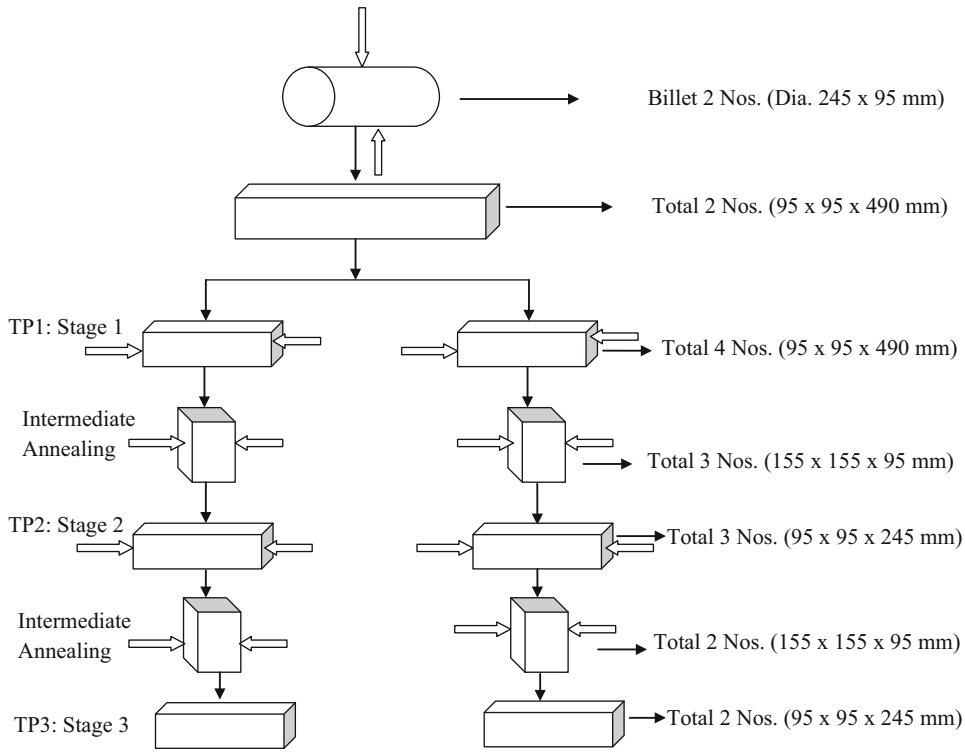

Note: Arrows indicate the thermomechanical working direction

Fig. 2 Schematic representation of forging operations carried out on AA7075 billets Arrows indicate the thermomechanical working direction

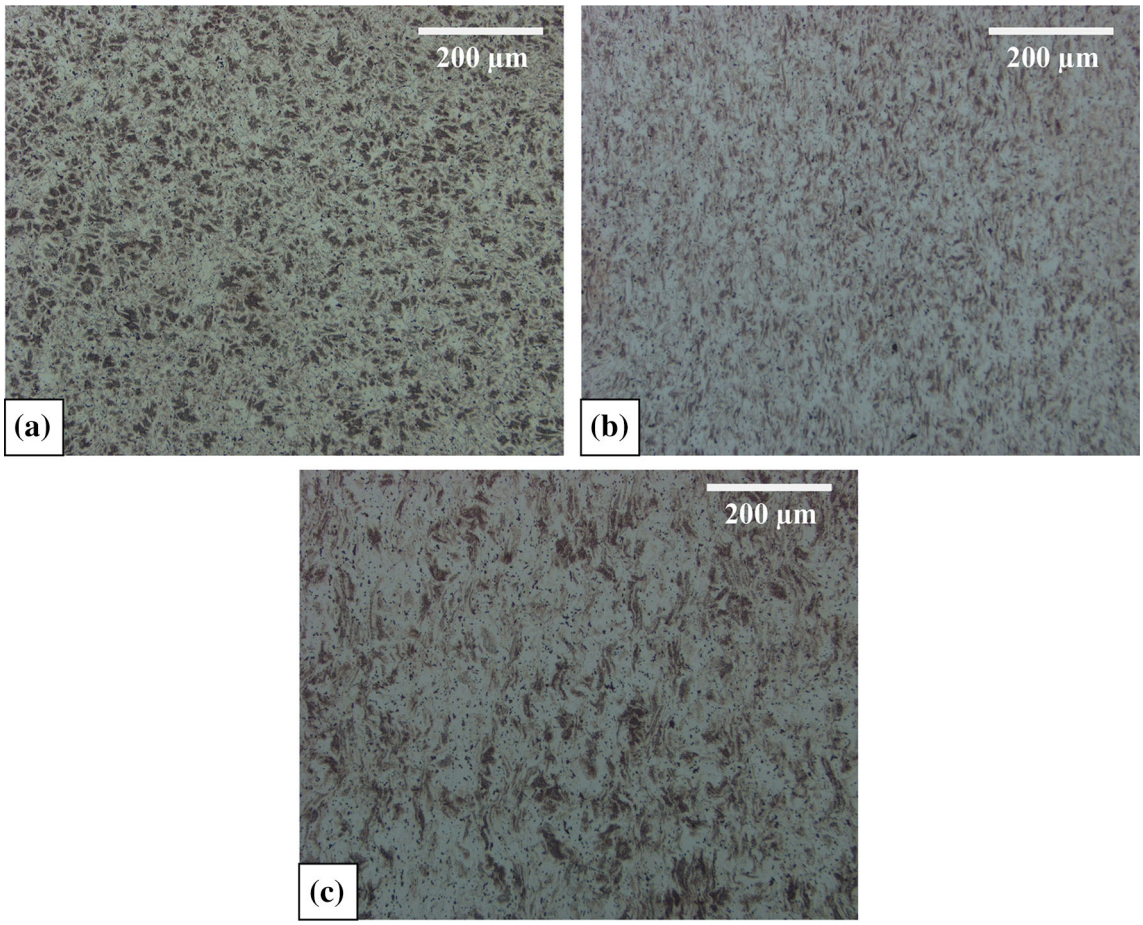

Fig. 3 Optical micrographs of (a) TP1, (b) TP2 and (c) TP3 in transverse directions

Transmission electron microscopy (TEM) was carried out to reveal the difference in grain boundary precipitates (GBPs) as a result of change in processing conditions. First, the alloy samples were dry polished to a thickness of 80-100 μm with a surface finish of 1200 grit SiC emery paper. From these thin foils, a disk of 3-mm diameter was punched out. This disk was polished by STRUERS make TenuPol-5 twin-jet electropolishing apparatus using 30 vol.% nitric acid and 70 vol.% methanol at −18 °C (9 V, 160-200 mA). The images obtained were taken on a JEOL make 2100F field emission gun transmission electron microscope (FEG-TEM) at 200 kV.

2.3 Potentiodynamic Polarization

The electrochemical corrosion of the alloy was evaluated through potentiodynamic polarization tests using a computer-controlled Zhaner IM6ex make electrochemical workstation. Samples were taken from the transverse direction of the forging to make specimens of 0.5 cm^2 area. The corrosion behavior of the forged alloy samples was examined in 3.5% NaCl solution prepared using reagent-grade NaCl salt and deionized water. The tests were carried out using a standard three-electrode setup with platinum as the counter electrode, saturated calomel electrode (SCE) as a reference, and the test specimens as working electrode. A scan rate of 0.5 mV/s was used. All the scans were started from a potential 300 mV below the corrosion potential (E_{corr}). Prior to the experiment, the samples were ground with SiC papers up to 1000 grit followed by cleaning in acetone and water.

2.4 Slow Strain Rate Test

Stress corrosion susceptibility of the samples was evaluated by the SSRT method as per ASTM G129 standard at a strain rate of 5×10^{-7} s^{-1}. The tests were performed in 3.5% NaCl and air as the corrosive and reference environments, respectively. SSRT was performed using a CORTEST make CERT tensile testing machine (CORTEST Inc, Willoughby, OH, USA). An acrylic container served as a cell to hold the specimen in the environment. The gage portion of the samples was polished using 600-grit SiC paper on all the sides to obtain a smooth surface. The average elongation of the specimen was measured by a pair of linear variable displacement transducers positioned on both sides of the specimen. Galvanic corrosion of the specimen and the grip material was avoided by using silicone rubber sealant to coat the interface between the specimen and the grip portions. The ratio of elongation at failure in the corrosive environment to that in air $\varepsilon_{(NaCl)}/\varepsilon_{(air)}$ was used as a measure to assess the SCC susceptibility.

3. Results and Discussion

3.1 Microstructures

3.1.1 Optical Microscopy. The microstructure of the as-cast homogenized sample of AA7075 generally contains phases such as η ($MgZn_2$), S (Al_2CuMg), β (Mg_2Si), and the ternary phase Al_7Cu_2Fe (Ref 13). It may be noted that these phases are

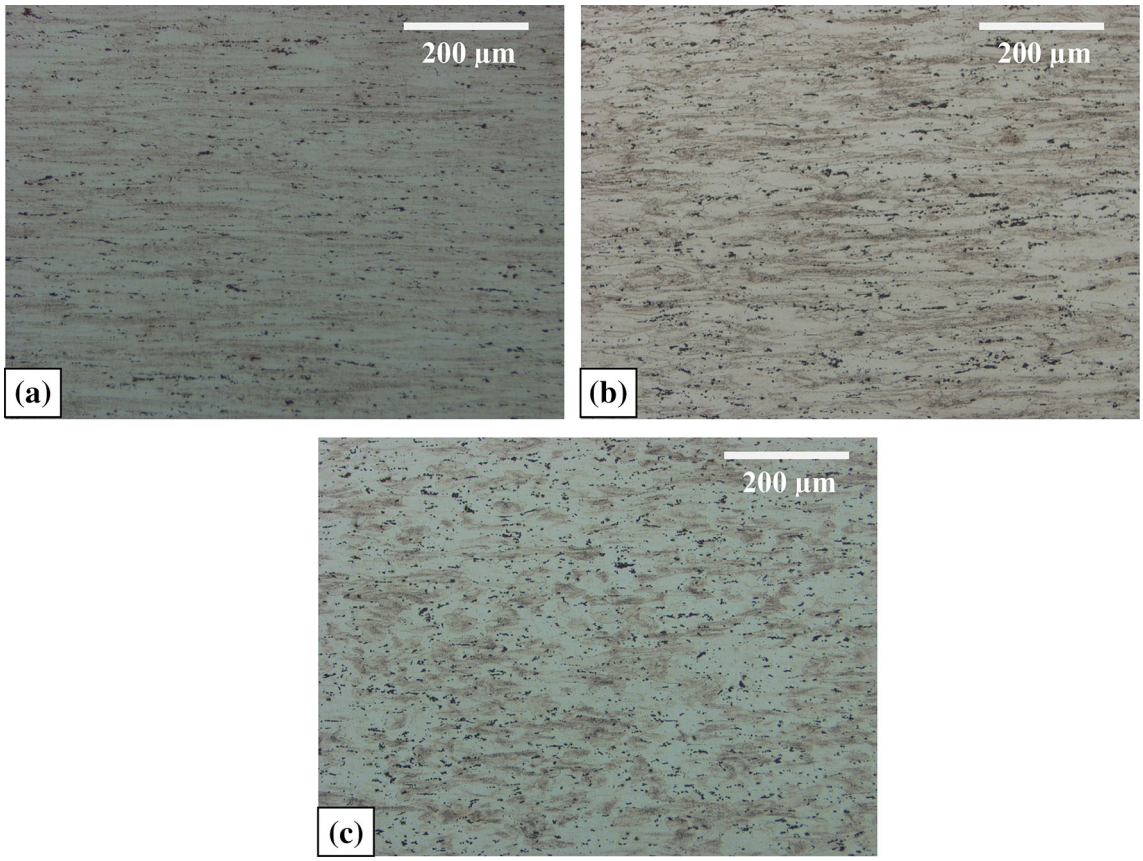

Fig. 4 Optical micrographs of (a) TP1, (b) TP2 and (c) TP3 in longitudinal directions

seen as coarse intermetallics in optical microscope at random location as shown in Fig. 1. Subsequent thermomechanical treatment aligns the particles in the working direction and is referred to as stringers. Solutionizing post thermomechanical treatment dissolves the phases such as η ($MgZn_2$), whereas it is unable to eliminate Fe-based phases (Al_7Cu_2Fe). The microstructures of the forged alloy samples corresponding to transverse and longitudinal directions after subjecting them to different thermomechanical treatments are shown in Fig. 3 and 4. Examination of the microstructure along the long transverse (LT) direction revealed remnant cast structure in TP1 which is gradually broken up as a function of working and the grain flow is clearly seen along the working direction for the samples TP2 and TP3 (Fig. 3). It can also be noted that insoluble intermetallic particles (Al_7Cu_2Fe, Al_2CuMg, Mg_2Si, etc) are found to be present along the grain boundaries as well as within the matrix as shown in Fig. 4 (Ref 4, 5).

Comparison of the microstructures in Fig. 4 shows that the alloy has undergone good working as seen from the well-elongated grains. The longitudinal view of the base alloy TP3 shows network of small recrystallized grains as well as the original elongated grains in contrast to microstructure of TP1 and TP2, even though the alloy (TP3) is sufficiently worked. This could be due to multiple annealing treatments imparted on the material during thermomechanical operations. It can also be observed that the second phase particles are found to be present discontinuously throughout the alloy and the directional pattern seen in TP1 and TP2 is absent. With respect to the size of the second phase particles, they are comparable in TP1 and TP2 and marginally increased in the case of TP3.

3.1.2 SEM-EDS. Elemental analysis was carried for TP1 out to measure the change in chemical composition across different areas (spectrum 1 and spectrum 2) as shown in Fig. 5. Spectrum 2 shows slightly higher Magnesium and Zinc content than spectrum 1. Also elemental analysis was carried out to measure the chemical composition of some of the insoluble intermetallic compounds present in the alloy after heat treatment. Spectrum 3 shows Al-Cu-Fe-based intermetallics near to stoichiometric composition Al_7Cu_2Fe particles present in the alloy as stringers and generally affect ductility of the alloy if not uniformly distributed by thermomechanical processing. The higher Zn and Mg contents would lead to chemical inhomogeneity which resulted in preferential attack during metallographic etching. This can be seen in the SEM picture as variation in contrast.

3.1.3 Transmission Electron Microscopy (TEM). The bright field TEM images corresponding to TP1, TP2, and TP3 are presented in Fig. 6. Comparison of the micrographs revealed that the precipitates are found to be coarser in TP1 and TP3 and little coarser in the case of TP2. Since the temper condition of the samples is same except the percentage of working imparted during stages, the representative selected area diffraction pattern (SADP) in Al $<110>$ projection is also shown in Fig. 6e. The SADP for the alloy in T7352 temper reveals several spots from the equilibrium precipitate η and less from η′. Absence of any diffuse streaks in SADP indicates that the alloy is in T7352 condition, typical of overaged condition (Ref 14). These precipitates are essentially η with η′ precipitates present in a smaller extent. TEM micrographs of the alloy in T7352 temper condition show coarse precipitates with

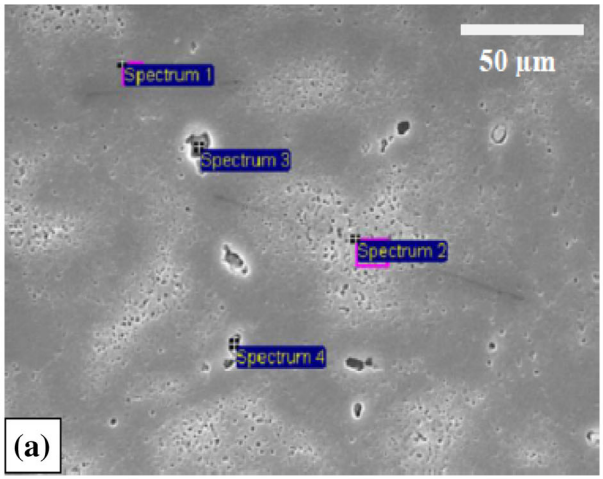

	Spectrum 1	Spectrum 2	Spectrum 3	Spectrum 4
Mg,%	2.47	2.63	0	0
Al,%	90.57	90	62.6	60.39
Cu,%	1.24	1.15	28.57	39.61
Zn,%	5.72	6.23	0	0
Fe,%	0	0	8.83	0
Total,%	100	100	100	100

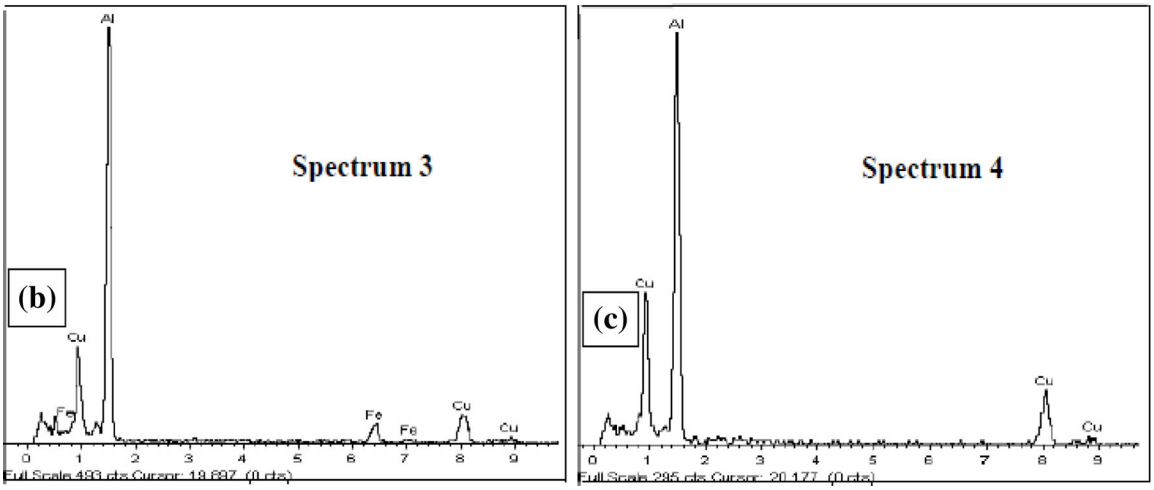

Fig. 5 (a) SEM micrograph of the specimen TP1 showing locations for EDS analysis, (b) and (c) showing peaks for spectrum 3 and spectrum 4

uniform distribution inside the grains. Precipitate-free zones (PFZ) are also formed due to depletion of solute either side of the grain boundary owing to overaging temper. The findings are in close agreement with the other published literatures (Ref 14-16). It may also be noted that except for volume fraction/size of the η′ precipitates, the microstructure is similar and the electrical conductivity is above 40% IACS (International Annealed Copper Standard) for all the samples (TP1, TP2, and TP3), typical of T7352 temper. When the volume fraction of the η′ is higher, precipitates are finer in TP2 and the sample has shown higher yield strength.

Thermomechanical working improves the homogeneity of the material and decreases the percentage of remnant cast structure to minimum level (Ref 17); hence the response to further heat treatment is enhanced. The intermediately worked structure (TP2) shows better responses to the T7352 temper than the other two samples, which is evident from the bright field imaging of the sample.

3.2 Tensile Properties

The tensile properties obtained for TP1, TP2, and TP3 are shown in Table 1. The reported values are the average of the tests done in triplicate.

An examination of the table shows that the alloy TP3 exhibited lower mechanical strength than the other experimental alloys. With respect to elongation, TP1 has lower value than TP2 and TP3. The average LT tensile and 0.2% YS values of over aged AA7075 alloy as per AMS specification (AMS 4147 D) are 434 and 345 MPa, respectively. Comparison of the specified properties with that of TP1 demonstrates that they are just meeting (440 and 347 MPa). But the same were much lower (414 and 331 MPa) for TP3. Although TP1 exhibits adequate strength to meet the specified values in spite of less working, the El.% is still lower (10.5) than TP2 (11.5) and TP3 (14.1). This shows that intermediately worked structure TP2 has a better response to heat treatment owing to the higher mechanical properties.

Despite the improvement in the microstructure, the poor mechanical strength of TP3 can be attributed due to the formation of undesirable coarse precipitates as evident from the optical and TEM microstructures. All these changes exhibited a typical highly over aged condition. These changes were caused by the additional pre-heating steps given to the alloy before hot working. Hence, optimum working with limited pre-heating is needed to obtain the desired mechanical properties. This is evidently seen from the results of experimental alloy TP2 wherein the fine and uniform distribution of precipitates resulted in higher mechanical properties. The results obtained in the present study show that the thermomechanical treatment of AA7075 aluminum alloy during billet processing influences

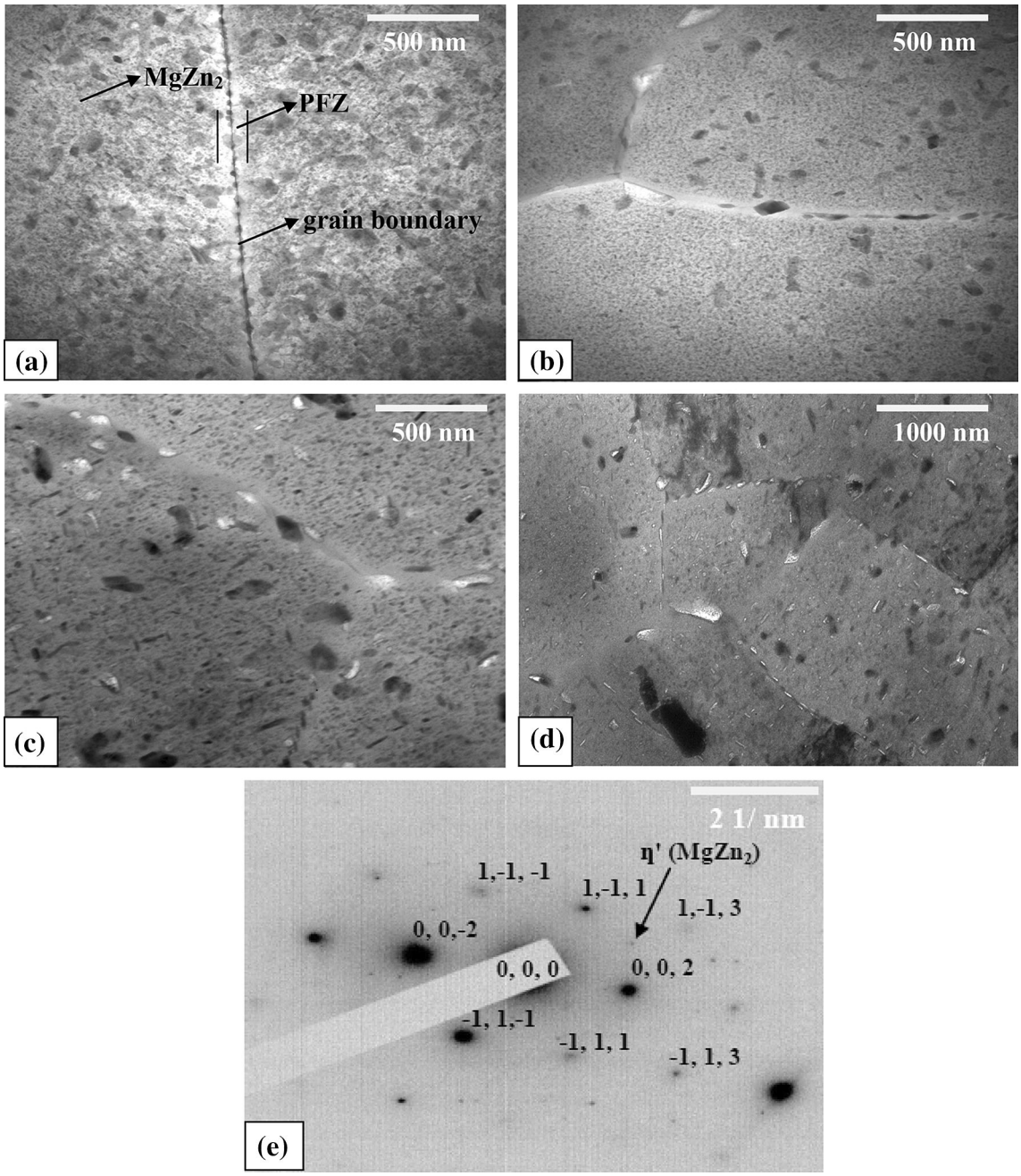

Fig. 6 Bright field TEM images of (a) TP1, (b) TP2, (c) TP3, (d) TP3 showing grain boundary precipitates, precipitate-free zones and the size of the matrix precipitates and (e) representative selected area diffraction pattern (SADP) of AA7075 alloy in T7352 condition in Al <110> projection

Table 1 Mechanical properties of AA7075-T7352 in TP1, TP2, TP3 conditions

		Transverse	Longitudinal
TP1	0.2% Proof stress, MPa	347	378
	Ultimate tensile strength, MPa	440	446
	Elongation after fracture, %	10.5	13.1
TP2	0.2% Proof stress, MPa	364	389
	Ultimate tensile strength, MPa	456	458
	Elongation after fracture, %	11.5	14.6
TP3	0.2% Proof stress, MPa	331	338
	Ultimate tensile strength, MPa	417	425
	Elongation after fracture, %	14.1	14.0

the quality of the alloy forging in two ways. Firstly, inadequate working resulted in poor response to heat treatment leading to lower mechanical properties. Although the grain flow and homogeneity of the material were significantly improved by further working (Fig. 3), the mechanical properties (UTS and 0.2% YS) were deteriorated especially under sufficiently worked condition. These changes were apparently seen from the tensile test results obtained for the three experimental alloys TP1, TP2, and TP3.

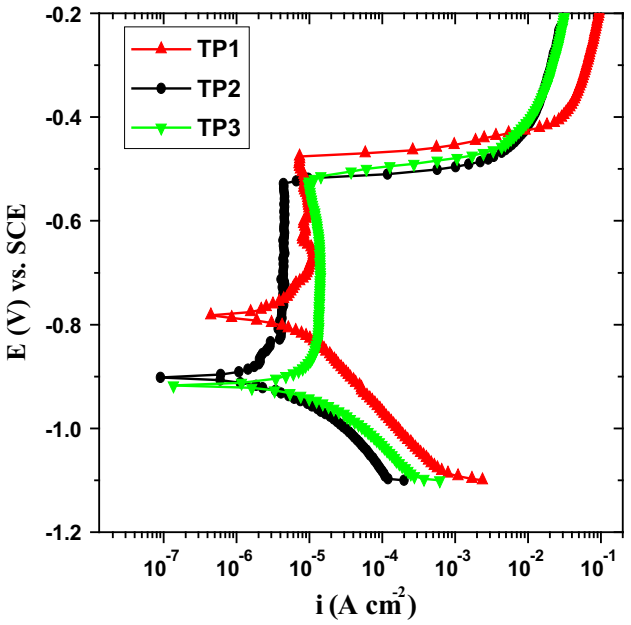

Fig. 7 Potentiodynamic polarization plots for TP1, TP2, TP3 in 3.5 wt.% NaCl solution

3.3 Potentiodynamic Polarization

The electrochemical corrosion of the TP1, TP2, TP3 samples is shown in Fig. 7. The key electrochemical parameters derived from the polarization curves are listed in Table 2. The corrosion morphology of the samples observed after polarization tests is represented in Fig. 8. The polarization curves in general exhibited some passivity for all the samples. However, the passive current was found to be fluctuating for TP1 when compared to TP2 and TP3. The absence of stable passivity for TP1 is due to the remnant cast structure. The elemental analyses by SEM-EDS revealed the elemental variation across the areas (spectrum 1 and spectrum 2). These areas are expected to undergo preferential corrosion as these elements are active when compared to aluminum. The morphology of corrosion attack as seen in the SEM photographs revealed that the attack tended to proceed along these areas. As

Table 2 Electrochemical parameters obtained from the polarization plots

Sample	E_{corr}, (V) vs SCE	i_{corr}, μA/cm^2	i_{pass}, μA/cm^2
TP1	−0.78	7.8	10.0
TP2	−0.91	4.0	6.0
TP3	−0.92	12.0	30.0

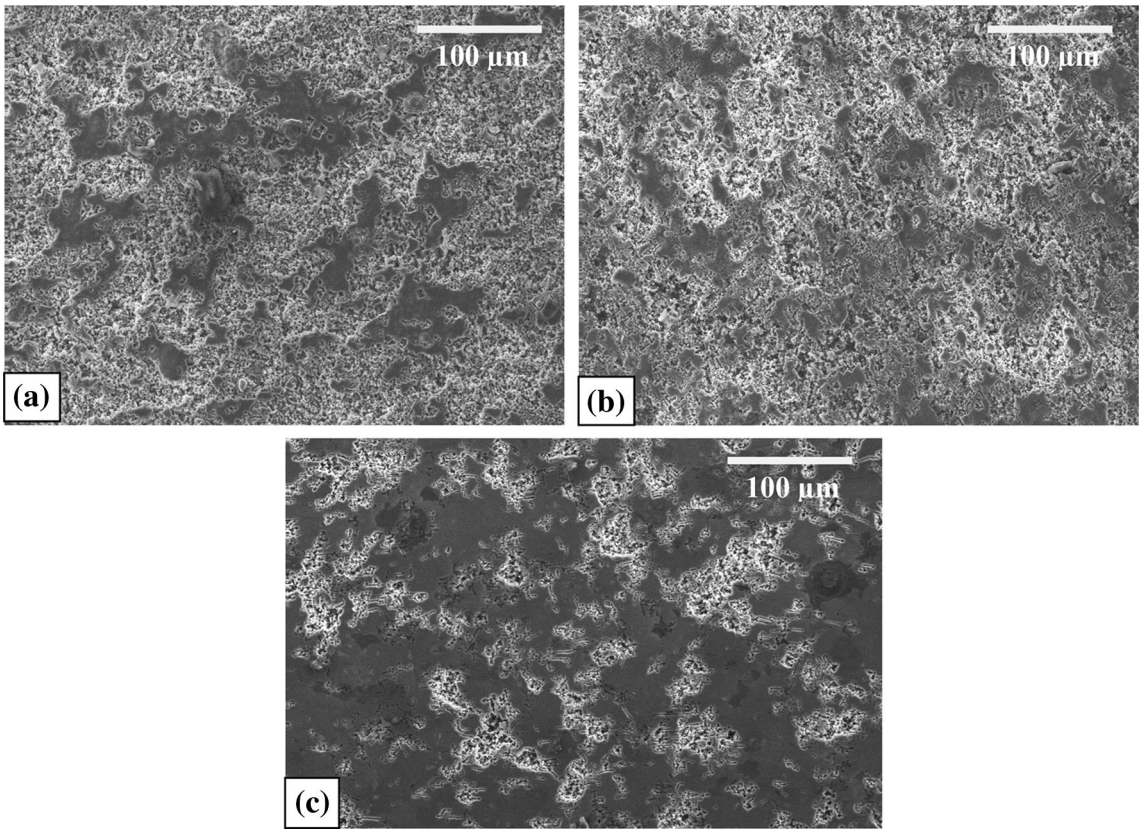

Fig. 8 SEM images of the potentiodynamic polarized samples of (a) TP1, (b) TP2 and (c) TP3

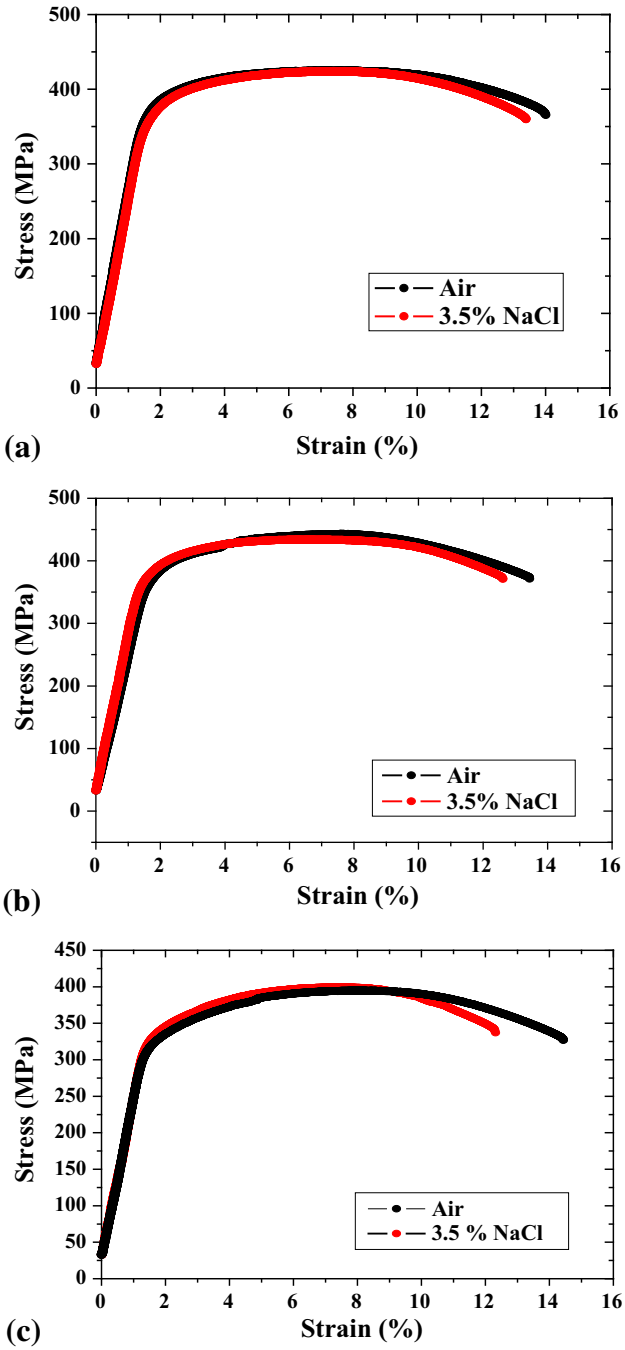

Fig. 9 SSRT results in the form of stress vs. % strain plot for AA7075 in air and 3.5% NaCl solution for (a) TP1, (b) TP2 and (c) TP3

a result of remnant cast structure, the measured i_{corr} of TP1 is higher than TP2. Since the microstructure was more homogenous in the case of TP2, the passive current density as well as i_{corr} was found to be very low. Although the extent of thermomechanical working was more for TP3, the microstructural refinement (reduction in remnant cast structure) could not improve the corrosion resistance of TP3 as it resulted in a highly over aged condition with large number of coarse precipitates resulting in higher corrosion rate. Two-fold increases in i_{corr} were seen for TP3 when compared to TP2. The corrosion morphology further indicates that the attack was found to be shallow in the case of TP1 and TP2, whereas the attack was found to be deep in the case of TP3.

3.4 Slow Strain Rate Tests (SSRT)

Figure 9 compares the stress-strain curves obtained for TP1, TP2, and TP3 samples in air and 3.5% NaCl solution, respectively. The SSRT data such as UTS, El.%, and SCC index (SI) measured from the stress-strain plots are summarized in Table 3. An examination of the stress-strain plots showed that the ductility of the samples was not affected significantly for TP1 and TP2 as a result of exposure to environment. However, in the case of TP3, there is a reduction in elongation for the environment tested samples when compared to the values measured in air. Furthermore, significant drop in the mechanical strength (UTS) can be noted for TP3 than that of TP1 and TP2. In this study, SI (ξ_{NaCl}/ξ_{air}) was used to evaluate the SCC resistance of all the samples, which is the ratio of the elongation of the samples tested in 3.5% NaCl solution and the air. The greater the SI value, the better the SCC resistance. An index value of unity implies that the material exhibits no SCC susceptibility. As a result of reduction in elongation in environment, the measured SI was low (0.87) for TP3 when compared to TP1 and TP2 (0.97). This indicates that TP3 is susceptible to SCC, whereas TP1 and TP2 are highly resistant to SCC. However, post test observation of the samples under stereo microscope after SSRT revealed large number of microcracks and pits within the gage length of the sample especially for TP3 tested in environment as shown in Fig. 10. For TP1 and TP2, the number of microcracks was less when compared to TP3. In the case of samples tested in air, no microcracks were seen and are similar for all the samples.

3.5 Fracture Morphology

An examination of the fracture surfaces observed under SEM after SSRT revealed a typical ductile cracking morphology for both air and NaCl environment tested samples as shown in Fig. 11. Also intergranular microvoid coalescences were found in all the samples after SSRT. This can be explained based on the preferential deformation of the PFZ around the grain boundary area. Clear ductile dimples with lots of plastic deformation of the material between dimples. Many of the dimples show a defect in the centre of the dimple which may have been responsible for the dimple formation. The grains were elongated for TP1 and TP2, whereas the fracture surface of TP3 shows less elongation of the deformed grains owing to partial recrystallization which is evident from the optical micrograph (Ref 18, 19). Hence the alloy subjected to different thermomechanical treatments is not susceptible to SCC in spite of the some microstructural variations. Close observation of the fracture surface of the TP3 sample tested in 3.5% NaCl revealed many localized corrosion in the form of pits. The stereo examination of the failed samples also showed numerous microcracks and localized corrosion. Hence, the reduction in elongation of the TP3 samples in NaCl can be attributed due to the localized pitting and that assisted the nucleation of cracks. The microstructural changes such as partial recrystallization and coarser precipitates are responsible for the reduction in mechanical properties and localized corrosion resistance of TP3, although the alloy had undergone sufficient working when compared to other samples. Hence the drop in SI (0.87) was due to electrochemical effect leading to pure mechanical cracking rather than true SCC. For other samples TP1 and TP2,

Table 3 Mechanical parameters obtained from SSRT in 3.5% NaCl

Sample		UTS, MPa	Elongation, %	SCC index
TP1				
	Air	426	13.4	0.98
	NaCl	421	13.1	
TP2				
	Air	440	11.0	0.97
	NaCl	438	10.7	
TP3				
Air		392	13.7	0.87
	NaCl	390	11.9	

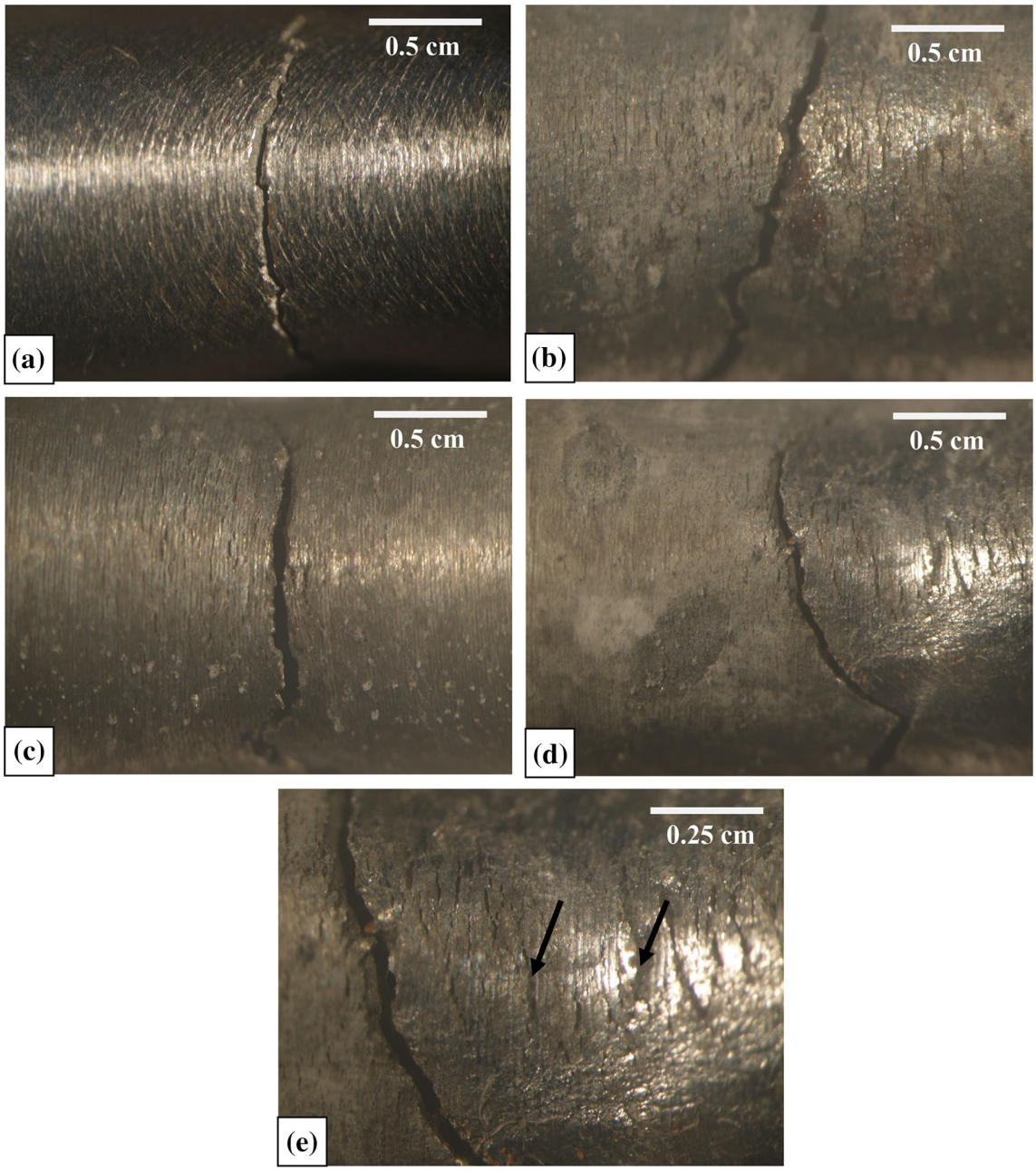

Fig. 10 Stereo photographs of fractured SSRT specimens showing extent of attack under (a) in air and (b) TP1, (c) TP2, (d) TP3: 0.50 cm and (e) TP3: 0.25 cm in 3.5% NaCl solution

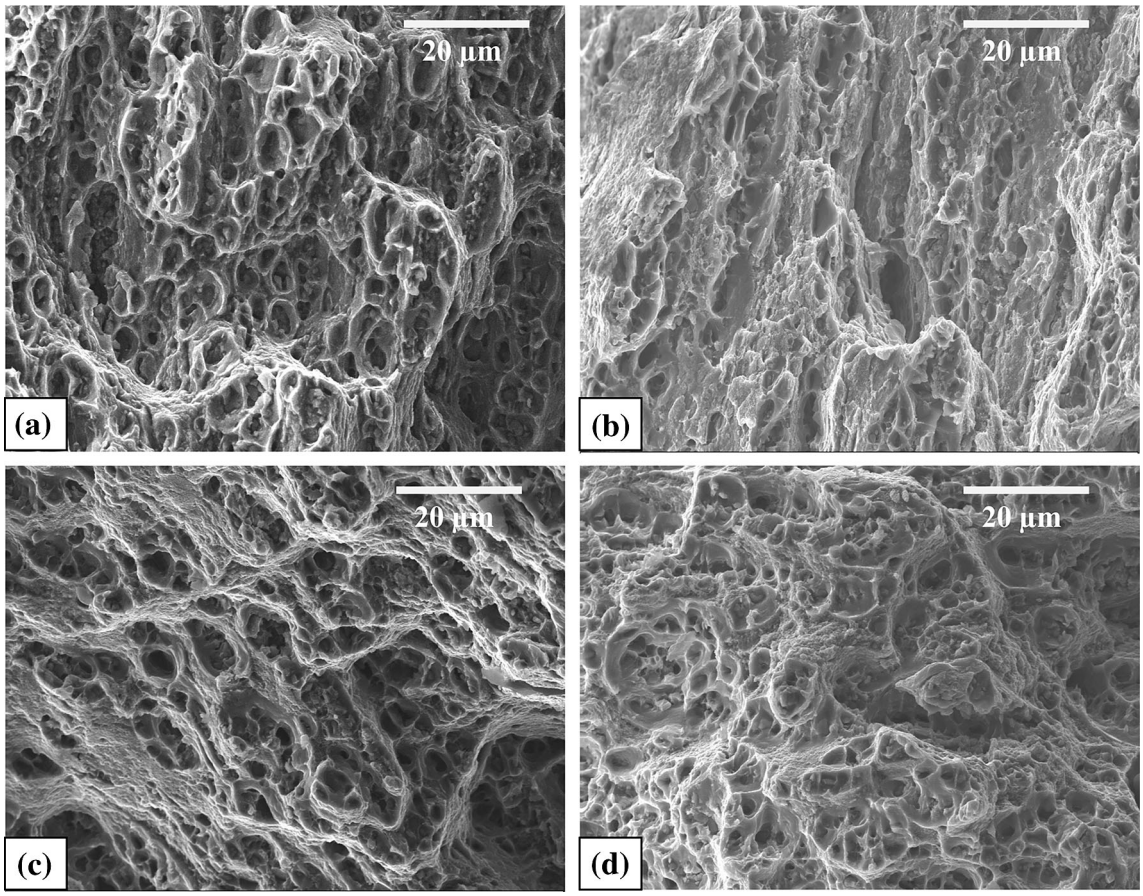

Fig. 11 Fracture morphology of the specimens after SSRT in (a) air and (b, c, d) NaCl for TP1, TP2, and TP3, respectively

the high SI values (0.97) along with predominantly ductile cracking morphology only indicate that they exhibited good localized corrosion resistance.

Hence microstructural observations and the SSRT properties are in line with the reported results of over aged AA7075 aluminum alloys. Results on the influence of thermomechanical treatment similar to the treatment followed in the present work are not available in the literature so as to compare the present results with the reported one. However, it was reported that intermediate thermomechanical treatment resulted in inferior fatigue properties of AA7050 alloy due to the effect of partial recrystallization during hot-rolling precipitation of undesirable Al_2CuMg particles during furnace cooling after hot rolling (Ref 6). Since the experimental alloy TP3 was subjected to two times annealing prior to hot forging, it is possible that the volume fraction of these particles is more in this sample. Hence the observed mechanical properties and corrosion resistance were low. The solution treatment cannot dissolve these particles completely. These particles tend to be present randomly as the hot forging aids in the mechanical redistribution of these particles during each stage.

In another study, it is reported that recrystallized grains are indeed more prone to SCC for AA7010 alloy in peak-aged condition (Ref 7). In the present work, even though the TP3 sample suffered partial recrystallization with coarse precipitation, the SI value was high (0.87) due to the over aged condition with discontinuous grain boundary precipitation. This indicates that over aging definitely improved the stress corrosion resistance of AA7075 alloy, although the mechanical properties are lower cautioning strict control over thermomechanical processing during billet processing.

4. Conclusions

Aerospace aluminum alloy components realized through forging route especially in the case of large scale billet involve multistage working with more pre-heating operations. Inadequate working may lead to the presence of remnant cast structure and sufficiently working may result in heterogeneous precipitation which negatively influences the mechanical and corrosion properties of the alloy. This work examined the electrochemical corrosion and environmental cracking resistance of AA7075 alloy forging after varying the extent of thermomechanical working and the significant findings are given below:

(1) AA7075 experimental alloy under inadequate working (TP1) and more than adequate working (TP3) resulted in inferior mechanical properties than the optimally worked condition (TP2). This was shown to be due to the presence of remnant cast structure and partially recrystallized grains along with coarse precipitates, for TP1 and TP3, respectively. As a result of this microstructural heterogeneity, the specified AMS (AMS 4147 D) mechanical properties could not be achieved especially for TP3.

(2) The heterogeneous microstructures also resulted in the higher corrosion rate of TP1 and TP3 when compared to TP2. The corrosion morphology of the samples observed after polarization tests evidently showed that the corrosion attack was predominantly through the remnant cast structure in TP1.
(3) In spite of the microstructural variations, the environmental cracking resistance of all the experimental samples was found to be good due to the size and spacing of the GBPs typical of over aged (T73) alloy and the measured SI values were high (0.97). The marginal reduction in elongation of the TP3 samples was shown to be due to localized pitting corrosion and not due to real SCC. The post test metallographic observation along with fracture morphology confirms the above findings.
(4) The results of this investigation in general suggest that effective billet processing using controlled working and pre-heating steps is needed to produce microstructures with optimum mechanical properties and SCC resistance.

Acknowledgments

The authors express their sincere thanks to Director, VSSC for permitting to publish the paper.

References

1. M.O. Speidel, Stress Corrosion Cracking of Aluminum Alloys, *Metall. Trans. A*, 1975, **6**, p 631–651
2. T.D. Burleigh, The Postulated Mechanisms for Stress Corrosion Cracking of Aluminum Alloys—A Review of the Literature 1980-1989, *Corrosion*, 1991, **49**, p 89–98
3. A.F. Oliveira, Jr., M.C. De Barros, K.R. Cardoso, and D.N. Travessa, The Effect of RRA on the Strength and SCC Resistance on AA7050 and AA7150 Aluminum Alloys, *Mater. Sci. Eng. A*, 2004, **379**(1-2), p 321–326
4. F. Andretta, H. Terryn, and J.H.W. de Wit, Effect of Solution Treatment on Galvanic Coupling Between Intermetallics and Matrix in AA7075-T6, *Corros. Sci.*, 2003, **45**, p 1733–1746
5. P.S. Pao, S. Gill, and L.R. Feng, On Fatigue Crack Initiation from Corrosion Pits in 7075-T7351 Aluminum Alloy, *Scr. Mater.*, 2000, **43**(5), p 391–396
6. N. Birbilis, M.K. Cvanaugh, and R.G. Buchheit, Electrochemical and Localized Corrosion Associated with Al_7Cu_2Fe Particles in Aluminum Alloy 7075-T651, *Corros. Sci.*, 2006, **48**, p 4202–4215
7. J. Wloka, G. Burklin, and S. Virtanen, Influence of Second Phase Particles on Initial Electrochemical Properties of AA7010-T76, *Electrochem. Acta*, 2007, **53**, p 2055–2059
8. R.P. Wei, C.M. Liao, and M. Gao, A Transmission Electron Microscopy Study of Constituent Particle Induced Corrosion in 7075-T6 and 2024-T3 Aluminum Alloys, *Metall. Trans. A*, 1998, **29**, p 1153–1160
9. M. Gao, C.R. Feng, and R.P. Wei, An Analytical Electron Microscopy Study of Constituent Particles in Commercial 7075-T6 and 2024-T3, *Metall. Trans. A*, 1998, **29**, p 1145–1152
10. J.E. Hatch, Ed., *Aluminum: Properties and Physical Metallurgy*, ASM, Metals Park, OH, 1984
11. C. Mondal, A.K. Singh, A.K. Mukhopadhyay, and K. Chattopadhyay, Evolution of Different Modes of Hot Cross-Rolling AA7010 Aluminum Alloy: Part I-Evolution of Microstructure and Texture, *Metall. Mater. Trans. A*, 2013, **44**, p 2746–2763
12. C. Mondal, A.K. Singh, A.K. Mukhopadhyay, and K. Chattopadhyay, Tensile Flow and Work Hardening of Hot Cross Rolled AA7010 Aluminum Alloy Sheets, *Mater. Sci. Eng. A*, 2013, **577**, p 87–100
13. D.K. Xu, N. Birbilis, D. Lashansky, P.A. Rometsch, and B.C. Muddle, Effect of Solution Treatment on the Corrosion Behaviour of Aluminium Alloy AA7150: Optimisation for Corrosion Resistance, *Corros. Sci.*, 2011, **53**, p 217–225
14. G. Sha and A. Cerezo, Early-Stage Precipitation in Al-Zn-Mg-Cu Alloy (7050), *Acta Mater*, 2004, **52**, p 4503–4516
15. G. Sha and A. Cerezo, Characterization of Precipitates in an Aged 7xxx Series Al Alloy, *Surf. Interface Anal.*, 2004, **36**, p 564–568
16. R. Ranganath, V. Anil Lumar, V.S. Nandi, R.R. Bhatt, and B.K. Muralidhara, Multi-stage Heat Treatment of Aluminum Alloy AA7049, *Trans. Nonferrous Met. Soc. China*, 2013, **23**, p 1570–1575
17. A.K. Jha, V. Diwakar, K. Sreekumar, and M.C. Mittal, Cracking of AFNOR 7020 Aluminum Alloy Component: A Metallurgical Investigation, *Eng. Fail. Anal.*, 2006, **13**, p 1233–1239
18. D. Wang, D.R. Ni, and Z.Y. Ma, Effect of Pre-strain and Two-Step Aging on Microstructure and Stress Corrosion Cracking of 7050 Alloy, *Mater. Sci. Eng. A*, 2008, **494**, p 360–366
19. M. Bobby Kannan and V.S. Raja, Enhancing Stress Corrosion Cracking Resistance in Al-Zn-Mg-Cu-Zr Alloy Through Inhibiting Recrystallization, *Eng. Fract. Mech.*, 2010, **77**, p 249–256